CFD-based Evaluation of Drag Force on a Sphere Unsteadily Moving Perpendicularly toward a Solid Surface: a Simple Model of a Biological Spring, *Vorticella Convallaria*

Sangjin Ryu[*1] and Paul T. Matsudaira[2]
[1]Department of Mechanical Engineering, [2]Department of Biology and Bioengineering, Massachusetts Institute of Technology
[1,2]The Matsudaira Laboratory, Whitehead Institute for Biomedical Research
*Corresponding author: 9 Cambridge Center, Suite 639, Cambridge, MA 02142, ryusj@mit.edu

Abstract: *Vorticella convallaria*, a sessile peritrich ciliate having a contractile stalk, is regarded as a model biological spring because of its remarkably fast contraction. Because the cell body shrinks to sphere-like shape during contractions, it can be assumed to be a sphere moving in quiescent water, and *Vorticella*'s contraction force has been evaluated with Stokes' law. However, flow induced by contracting *Vorticella* is unsteady and bound, and its Reynolds number reaches beyond 1. Although it was recently suggested to include drag force components due to acceleration, effects of finite Reynolds number and the substrate have not been included yet. In this study, we evaluate the contraction force of *Vorticella* with CFD simulations assuming the body to be a sphere unsteadily moving perpendicularly toward a wall and show that effects of accelerated motion of the body and the substrate must be considered in evaluating the contraction force of *Vorticella*.

Keywords: *Vorticella convallaria*, biological spring, contraction force, unsteady drag force, wall effect

1. Introduction

In this study, unsteady water flow driven by a solid sphere moving with acceleration perpendicularly toward a solid surface is simulated for drag force evaluation. The study is inspired by contractions of *Vorticella convallaria*. *Vorticella* is a sessile peritrich which has a body and a contractile stalk. The animal is tethered to a surface with its stalk. When stimulated, the stalk helically coils retracting the body.

Figure 1 shows a contraction of *Vorticella*. The unicellular animal completes its contraction in less than 10 msec, and its maximum contraction speed reaches about 8 m/sec, which is equivalent to 1,800 body length/sec [1]. The spasmoneme, a contractile organelle inside the stalk, is regarded as a model biological spring for a bioinspired actuator because it generates force and power hundreds to thousands times greater than other well known cell motility mechanisms [2]. Hence, the contraction force is a key parameter to describe and understand contractions of *Vorticella*.

As shown in figure 1, the body also contracts during a contraction, and its shape can be regarded as a sphere. Because the inertia of the body is negligible compared with drag force, *Vorticella*'s contraction force can be equated to drag force exerted on the body. It is also assumed that any effect of the complex geometry of the coiled stalk is negligible. Assuming the cell body to be a sphere moving in quiescent water, Stokes' drag formula shown as equation 1 had been used to evaluate the contraction force of *Vorticella* [1, 3].

$$F_C \approx F_D = -6\pi\mu RU \qquad (1)$$

The above formula is valid for a steady creeping flow of a unbound fluid [4], but the water flow caused by contracting *Vorticella* does not satisfy these conditions. First, the body is

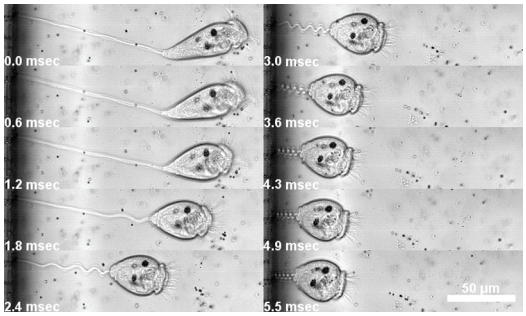

Figure 1. A contraction of *Vorticella convallaria*.

accelerated and decelerated during contractions, which results in unsteady flow. Second, as shown in figure 1, the body moves toward the substrate which obviously confines water and plays a role as no-slip wall condition. Last, the Reynolds number based on the body diameter and the maximum contraction speed is greater than 1. Therefore, the Stokes drag force obtained with equation 1 is a rough estimation of *Vorticella*'s contraction force.

A more rigorous evaluation of the contraction force should take account of any effects of accelerated motion of the body, the substrate and finite Reynolds number on drag force. Although Upadhyaya *et al*. introduced the unsteady drag force including the force due to added mass and the history force as shown as equation 2 in their contraction force estimation, they did not consider effects of the wall and finite Reynolds number [5, 6].

$$-F_D(t) = 6\pi\mu RU + \frac{2}{3}\pi R^3 \rho \frac{dU}{dt} + 6R^2\sqrt{\pi\mu\rho}\int_{-\infty}^{t} \left.\frac{dU}{dt}\right|_{t=\tau} \frac{d\tau}{\sqrt{t-\tau}} \quad (2)$$

The most rigorous estimation is possible with CFD simulations, which is the goal of this study. By comparing the simulation result with drag estimations based on the previous methods, we will show how significant effects are of accelerated motion of the body and the substrate. Although this study deals with a simple model of contracting *Vorticella*, a solid sphere unsteadily moving perpendicularly toward a solid surface, its methodology and result can be expanded to other similar fluid dynamic studies.

2. Experimental Method

The contraction velocity of *Vorticella* is required as a boundary condition for the simulation, so this contraction velocity was experimentally measured. *Vorticella* is cultured and harvested based on the method suggested by Vacchiano *et al*. [7]. After harvest, small fragments of cover glass were placed in a petri dish containing collected cells. Cells were allowed a day to attach to the glass fragments and grow their stalk.

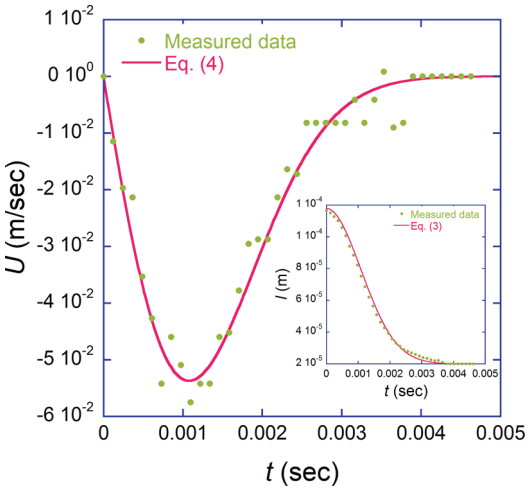

Figure 2. Contraction velocity curve and stalk end-to-end length curve (inset).

Because the stalk of a cell attaching to vertical sides of the glass fragment was parallel to the microscope stage, such a cell was chosen for measurement. Contractions of *Vorticella* were captured with a high-speed camera (Phantom V7, Vision Research, Wayne, NJ) and an inverted light microscope (Nikon Eclipse TE300, Nikon Instruments, Melville, NY) at 8,200 frames per second using a 40× objective lens. Image size is 512×512 pixels, and 1 pixel corresponds to 0.5 µm. The images were analyzed with MATLAB (Mathworks, Natick, MA). The end-to-end length of the stalk was measured by obtaining the *x*-*y* coordinates of both ends of the stalk, and the contraction speed was calculated based on the stalk length measurement.

Moriyama, Hiyama & Asai used a combination of a polynomial function and an exponential function to describe the time course of stalk length change [1]. Because their approach may have a problem of discontinuity in higher order derivatives, we used a single function instead. Having realized that the stalk length change shown in the inset of figure 2 resembles a Gaussian function, we employed an exponential function for the stalk length change and fitted its time derivative versus the measured contraction velocity by the method of least square. Equations 3 and 4 show the obtained fitting curves, and figure 2 shows that they agree well with the experimental data.

$$l = 9.7942\times10^{-5}\exp\left(\frac{t^{1.9691}}{-2.9139\times10^{-6}}\right) + 1.6008\times10^{-5} \quad (3)$$

$$U = -66.1862t^{0.9691}\exp\left(\frac{t^{1.9691}}{-2.9139\times10^{-6}}\right) \quad (4)$$

3. Numerical Model

3.1 Governing equation

Because the simple model is axial symmetric, the Navier-Stokes equation in the cylindrical coordinate system is the governing equation to be solved and is shown as equation 5. Using COMSOL Multiphysics, we combined the transient analysis solver of the incompressible Navier-Stokes equation and the transient analysis solver of ALE moving mesh mode. Drag force was calculated by integrating total z-direction force over the sphere's boundaries using **postint (fem, '2∗π∗R∗(T_z_ns)')**.

$$\begin{aligned}
&\rho\left(\frac{\partial u_r}{\partial t}+u_r\frac{\partial u_r}{\partial r}+u_z\frac{\partial u_r}{\partial z}\right)\\
&\quad=-\frac{\partial p}{\partial r}+\mu\left[\frac{1}{r}\frac{\partial}{\partial r}\left(r\frac{\partial u_r}{\partial r}\right)+\frac{\partial^2 u_r}{\partial z^2}-\frac{u_r}{r^2}\right]\\
&\rho\left(\frac{\partial u_z}{\partial t}+u_r\frac{\partial u_z}{\partial r}+u_z\frac{\partial u_z}{\partial z}\right)\\
&\quad=-\frac{\partial p}{\partial z}+\mu\left[\frac{1}{r}\frac{\partial}{\partial r}\left(r\frac{\partial u_z}{\partial r}\right)+\frac{\partial^2 u_z}{\partial z^2}\right]
\end{aligned} \quad (5)$$

3.2 Preliminary simulation

To test possible moving mesh methods, we created two cases of two-dimensional axial symmetric mesh with triangular elements as shown in table 1. The no-slip wall condition is assigned to boundary ⑤ representing the substrate, and the moving wall condition to boundaries ②③ corresponding to the sphere. In Mesh 2, the domain is split to two subdomains, and boundary ⑨, the border between the subdomains, moves along with the sphere part at the same speed. To reduce deformation of elements, we set boundaries ①④ of Mesh 1 and boundaries ①④⑥⑦ of Mesh 2 to shorten or lengthen linearly based on the curve parameter **s** corresponding to the sphere's movement.

Table 1: Preliminary simulation models.

Mesh 1	Mesh 2
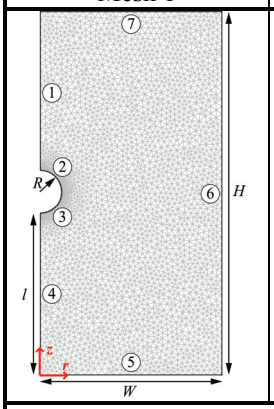	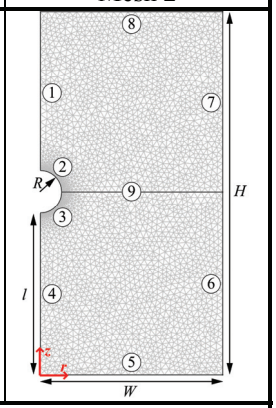

Boundary condition	
Axial symmetry condition	①④
Moving wall condition	②③
No-slip wall condition	⑤
Open boundary (Normal stress, f_o= 0)	Mesh 1:⑥⑦ Mesh 2:⑥⑦⑧
Moving interior boundary	Mesh 2: ⑨

Mesh dimension			
W	128 μm	R	15.3 μm
H	256 μm	l	113.95 μm

Because the quality of the mesh is critical in CFD simulations, we tried three moving mesh methods as figure 3 shows. The first case using Mesh 1 does not have any special treatment for deformed elements, so elements around the sphere part are expected to undergo severe deformation. The second case also employs Mesh 1, but it is different in that the mesh is automatically remeshed with the same element size every 0.5 msec. The last time step solution of the old mesh is mapped to the new one as the initial condition. The final case uses Mesh 2 which has a moving interior boundary. Elements of the top and bottom subdomain are elongated and compressed in the z-direction, respectively. In all cases, flow was simulated for 10 msec with a time step of 0.01 msec.

Figure 3 shows drag force calculation results with pressure distribution and streamlines at 0.5, 1.0 and 10 msec. In Case 1, inverted elements first appeared at 1.48 msec, and they are found near the stagnation point of the sphere. Severely deformed elements seem to have caused

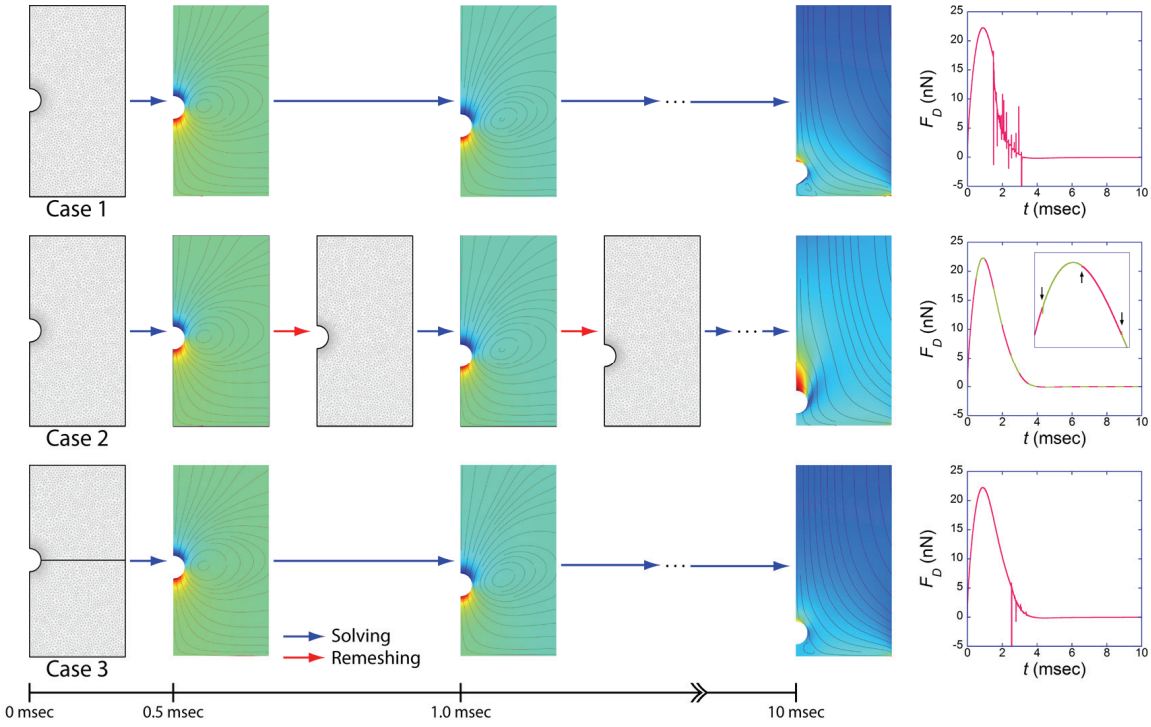

Figure 3. Three methods of moving mesh and their drag force calculation results.

fluctuations in the drag force calculation. In contrast, Case 2 did not show any inverted elements owing to automatic remeshing, and its drag force calculation result is reasonable. However, the Case 2 result shows discontinuities at every time step when remeshing was done (arrows in the inset). Solution mapping seems to have caused these discontinuities. Even in Case 3, which was designed to minimize element deformation without remeshing, inverted elements were unavoidable because final gap distance is small ($\approx R$). Although some elements started to be reversed at 2.55 msec in Case 3, the moving interior boundary helped reducing severe deformation of elements.

3.3 Mapped mesh model

Considering the preliminary simulation results, we created a new mapped mesh employing rectangular elements and moving interior boundaries. Figure 4 shows the mesh, and the inset is a close-up of the sphere part. Assigned boundary conditions and dimensions are same as those of Case 1 except that W and H are 512 μm.

The mesh is divided into three subdomains. The middle subdomain, which is surrounded with the green box in figure 4, moves as a whole along the sphere part, and the other subdomains expand or contract accordingly in the z-direction as Case 3. For instance, boundary ⑥ consists of three segments, and the top and bottom one lengthens or shortens based on the curve

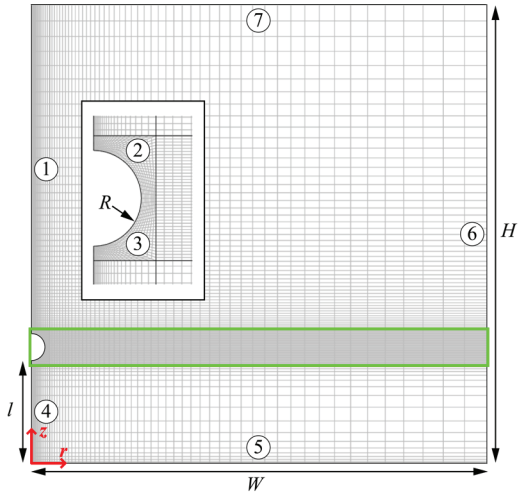

Figure 4. Mapped mesh with rectangular elements.

parameter **s**, respectively. This moving mesh strategy prevents any deformation of elements around the sphere part.

4. Results & Discussion

4.1 Model verification

To verify the simulation mesh, we simulated three flow cases and compare drag force obtained from the simulation with known results or exact solutions. The first case is steady flow passing by the stationary sphere. For this simulation, the no-slip wall condition was set for boundaries ②③, and the inlet velocity condition for boundary ⑤. Drag coefficients obtained from the simulation are compared with Schiller-Nauman formula, a standard drag correlation which is valid for Re < 800, shown as equation 6 [6]. As figure 5 shows, the simulation results are in a good agreement with the formula.

$$C_D = \frac{24}{\mathrm{Re}}\left(1 + 0.15\,\mathrm{Re}^{0.687}\right) \tag{6}$$

As the second case, the sphere part of the model was set to move toward the wall at constant velocity. In this case, the exact solution of drag force is given as equation 7, and it is valid when $l > R$ and Re << 1 [8]. The wall effect correction factor λ was calculated by dividing simulation-based drag force with the Stokes drag force. Figure 6 shows that simulation results agree well with the exact solution for Re < 1. Because the sphere starts moving suddenly in the simulations, the obtained correction factor shows deviation from the exact solution at the beginning of the sphere's movement.

$$F_D = -6\pi\mu R U \lambda$$

$$\alpha = \cosh^{-1}\left(\frac{l+R}{R}\right) \tag{7}$$

$$\lambda = \frac{4}{3}\sinh\alpha \sum_{n=1}^{\infty} \frac{n(n+1)}{(2n-1)(2n+3)} \times \left[\frac{2\sinh(2n+1)\alpha + (2n+1)\sinh 2\alpha}{4\sinh^2(n+1/2)\alpha - (2n+1)^2\sinh^2\alpha} - 1\right]$$

In the last case, the sphere part was set to oscillate in the z-direction according to velocity

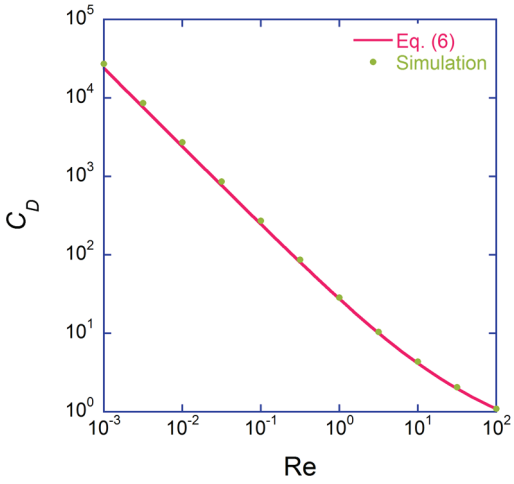

Figure 5. Steady drag coefficient comparison.

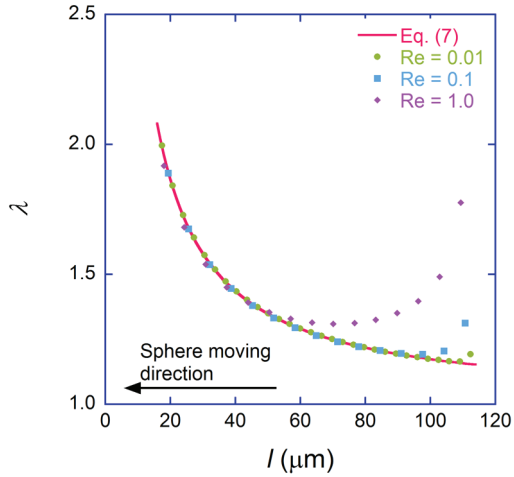

Figure 6. Wall effect correction factor comparison.

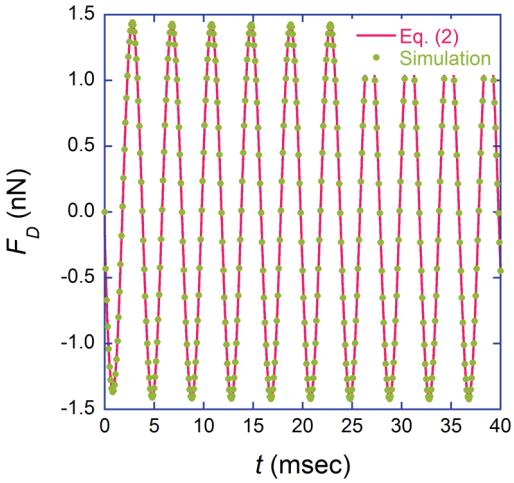

Figure 7. Unsteady drag force comparison.

given as equation 8. In figure 2 the contraction velocity of *Vorticella* reaches its minimum at around 1 msec, so the oscillation period was chosen to be 4 msec. In case of Re << 1, drag force on the oscillating sphere can be calculated with equation 2. The simulation result and unsteady drag force obtained with equation 2 show a good agreement up to Re = 1. Figure 7 shows the result of Re = 0.1.

$$U = \mathrm{Re}\frac{\mu}{2\rho R}\sin\left(2\pi\frac{t}{0.004}\right) \qquad (8)$$

4.2 Contraction force evaluation

After the simulation mesh was verified as shown in the previous section, we evaluated the contraction force of *Vorticella*. The contraction velocity expressed with equation 4 was assigned for the boundaries corresponding to the sphere (or the cell body), and water flow caused by the sphere was simulated for 10 msec with a time step of 0.01 msec. In contrast to the preliminary simulation, there was no inverted element.

Figure 8 shows the simulation-based drag force as well as the Stokes drag force obtained with equation 1 and the unsteady drag force obtained with equation 2. While the Stokes drag force reaches its maximum value of 15.5 nN at 1.07 msec, the unsteady drag force and the simulation-based drag force have maximum values of 21.9 nN and 22.5 nN at 0.86 msec and 0.89 msec, respectively. Stokes' drag formula underestimates the maximum drag force by about 30% compared with the others. This is mainly due to the history force. According to Upadhyaya *et al*., the history force accounts for about 20 % of the total force generated by *Vorticella* before it achieves the maximum contraction speed [5]. Seeing the excellent agreement between the current simulation and the unsteady drag force formula, it is evident that the unsteady drag force components must be considered in evaluating the contraction force of *Vorticella*.

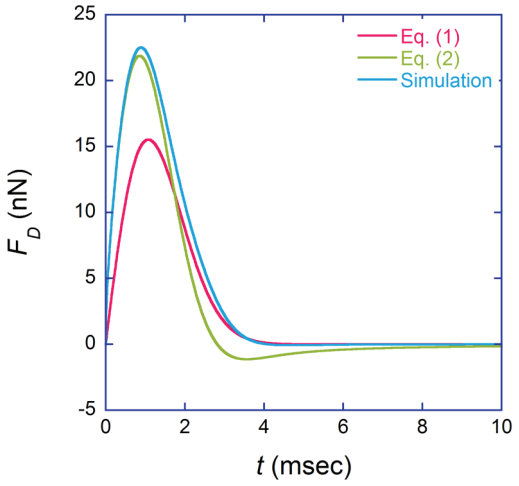

Figure 8. Drag force on contracting *Vorticella*.

On the other hand, it is noticeable that, according to the unsteady drag force formula, the sphere experiences negative drag force, which is in the direction of the sphere's movement, after 2.83 msec. This happens because water cannot stop flowing although the sphere almost stops moving. Although the current simulation confirms that water keeps flowing while the sphere effectively has stopped, however, resultant negative drag force is negligible. This difference is due to the substrate. Because the following water flow is blocked by the wall and it has no driving energy source any longer, it cannot exert significant drag force on the sphere. To check the wall effect, we ran the same simulation after changing the boundary condition of boundary ⑤ to open boundary condition and found that the simulation result shows a good agreement with the unsteady drag force (data not shown). Therefore, the effect of the substrate must be considered in evaluating the contraction force of *Vorticella*.

5. Conclusions

In this study we applied the CFD technique in evaluating the contraction force of a biological spring, *Vorticella convallaria*. The cell body was modeled as a solid sphere unsteadily moving perpendicularly toward a solid surface, and the corresponding two-dimensional axial symmetric model was created after preliminary simulations to find an appropriate moving mesh method. The model was tested to calculate the steady drag coefficient of the sphere, the wall effect correction factor and unsteady drag force on an oscillating sphere, and the results showed excellent agreements with known results or exact solutions.

For evaluation of *Vorticella*'s contraction force, experimentally measured contraction velocity was given as a boundary condition for

moving mesh. The simulation result agrees well with unsteady drag force, which consists of the quasi-steady drag force, the force due to added mass and the history force, until the maximum speed is reached. Maximum values of the simulation-based drag force and the unsteady drag force are greater than that of the Stokes drag force, and the history force seems to be responsible for the difference. According to the unsteady drag force formula, *Vorticella* experiences drag force in the direction of contraction in the later stage of its contraction, but our simulation shows that the force is negligible. The difference is due to the wall effect. Therefore, effects of accelerated motion of the cell body and the substrate must be considered in evaluating the contraction force of *Vorticella convallaria*.

6. Acknowledgements

This study is supported by the Institute for Collaborative Biotechnologies through grant DAAD19-03-D-0004 from the U.S. Army Research Office.

7. References

1. Moriyama, Y., Hiyama, S. & Asai, H., High-speed video cinematographic demonstration of stalk and zooid contraction of *Vorticella convallaria, Biophys. J.*, **74**, pp. 487-491 (1998)
2. Mahadevan, L. & Matsudaira, P., Motility powered by supramolecular springs and ratchets, *Science*, **288**, pp. 95-100 (2000)
3. Amos, W. B., Reversible mechanochemical cycle in the contraction of *Vorticella, Nature*, **229**, pp. 127-128 (1971)
4. Currie, I. G., *Fundamental mechanics of fluids*. 2nd ed., McGraw-Hill, New York (1993)
5. Upadhyaya, A., Baraban, M., Wong, J., Matsudaira, P., van Oudenaarden, A. & Mahadevan, L., Power-limited contraction dynamics of *Vorticella convallaria*: an ultra-fast biological spring, *Biophys. J.*, pp. 265-272 (2007)
6. Clift, R., Grace, J. R. & Weber, M. E., *Bubbles, drops, and particles*, Academic Press, New York (1978)
7. Vacchiano, E. J., Kut, J. L., Wyatt, M. L. & Buhse, H. E., A novel method for mass-culturing *Vorticella, J. of Protozo.*, **38**, pp. 608-613 (1991)
8. Brenner, H., The Slow Motion of a Sphere through a Viscous Fluid towards a Plane Surface, *Chem. Eng. Sci.*, **16**, pp. 242-251 (1961)

8. Nomenclature

C_D: Drag coefficient $\left(= \dfrac{|F_D|}{\rho U^2 / 2 \cdot \pi R^2} \right)$
F_C: Contraction force of *Vorticella convallaria*
F_D: Drag force
H: Height of mesh
l: Gap distance, stalk end-to-end length
λ: Wall effect correction factor
μ: Fluid viscosity
p: Pressure
ρ: Fluid density
r: Radial coordinate
R: Sphere radius, body radius
Re: Reynolds number $\left(= \dfrac{2\rho R|U|}{\mu} \right)$
t: Time
u_r: Radial velocity
u_z: Axial velocity
U: Contraction velocity of *Vorticella*, Moving velocity of the sphere
W: Width of mesh
z: Axial coordinate